# Spin-orbit torque induced magnetization dynamics and switching in a CoFeB/Ta/CoFeB system with mixed magnetic anisotropy

Stanisław Łazarski,[1,*] Witold Skowroński,[1,†] Krzysztof Grochot,[1,2] Wiesław Powroźnik,[1] Jarosław Kanak,[1] Marek Schmidt,[3] and Tomasz Stobiecki[1,2]

[1]*Institute of Electronics, AGH University of Science and Technology, Al. Mickiewicza 30, 30-059 Kraków, Poland*

[2]*Faculty of Physics and Applied Computer Science, AGH University of Science and Technology, Al. Mickiewicza 30, 30-059 Kraków, Poland*

[3]*Institute of Molecular Physics, Polish Academy of Sciences, ul. Smoluchowskiego 17, 60-179 Poznań, Poland*

(Received 25 June 2020; revised 22 March 2021; accepted 29 March 2021; published 15 April 2021)

Spin-orbit torque (SOT) induced magnetization switching in CoFeB/Ta/CoFeB trilayer with two ferromagnetic CoFeB layers exhibiting in-plane and perpendicular magnetic anisotropy (PMA), respectively, is investigated. Interlayer exchange coupling (IEC), measured using the ferromagnetic resonance technique is modified by varying thickness of the heavy metal Ta spacer ($t_{Ta}$). The evolution of the IEC with $t_{Ta}$ leads to different orientations of the magnetic anisotropy axes of two CoFeB layers: for $t_{Ta} > 1.3$ nm, magnetization prefers antiferromagnetic alignment, whereas for $t_{Ta} < 1.3$ nm, ferromagnetic coupling is measured. The magnetization state of the CoFeB layer exhibiting PMA is controlled by the spin-polarized current originating from the Ta layer in micrometer sized Hall bars. The SOT induced critical current density with Ta spacer thickness is presented, showing an increase with decreasing $t_{Ta}$, which coincides with the CoFeB coercive field dependence. In a narrow range of $t_{Ta}$ corresponding to the ferromagnetic IEC, the field-free SOT induced magnetization switching is achieved.

DOI: 10.1103/PhysRevB.103.134421

## I. INTRODUCTION

Conventional electronic devices based only on the electric charge are facing energy efficiency issues due to the use of high current densities needed to control the device state that dissipates a lot of heat. Moreover, digital data stored in the form of electric charge, for example, in dynamic and static random access memories are volatile and, thus, need periodic refreshment. Spintronic devices, on the other hand, use both charge and spin of the electron to process and store information. Magnetism-based spintronic elements are by nature nonvolatile and potentially more energy efficient, nonetheless, there is still a need for further development of magnetization control mechanisms [1]. Digital information can be encoded in the magnetization state of a nanoscale magnet in a nonvolatile way. Research on various control mechanisms has recently received extensive attention due to the demand for a scalable and low-energy write and read processes [2]. Outstanding developments have been made in switching magnetic tunnel junctions (MTJs) and spin-valve structures via spin-transfer torque (STT) [3,4], electric fields [5,6], and recently vastly explored spin-orbit torque (SOT) [7–9]. MgO-based MTJs with in-plane magnetic anisotropy have been initially proposed as a main building block of a memory unit due to its high tunneling magnetoresistance ratio [10] and current induced switching [11]. Unfortunately, in general, STT-based devices require high critical current densities ($J_C$) via a thin tunnel barrier for the magnetization switching and have the disadvantage of low thermal stability. Perpendicularly magnetized MTJs using both interface perpendicular magnetic anisotropy (PMA) [12–14] and shape anisotropy [15] have been proposed to enhance thermal stability and to reduce $J_C$, however, a MgO tunnel barrier can still degrade its own properties over time due to high switching currents. To overcome this problem, the SOT effect in which spin currents are generated in layers with high spin-orbit couplings, such as heavy metals (HMs) [16] and topological insulators [17] has been studied. The switching of the magnetization driven by SOT with PMA does not require such a high-$J_C$ tunneling through a MgO barrier [16]. In addition, SOT induced magnetization switching enables the magnetization reorientation in the subnanosecond regime [18]. Originally, an external magnetic field had to be applied to assist SOT switching in order to break the time-reversal symmetry. Although the need for an external field in device applications would not be practical, therefore, numerous alternatives have been proposed, such as coupling to the antiferromagnets [19–25] or to another ferromagnet [26,27], use of interface torques [28], combination of STT and SOT effects [29], or using a dipolar field from an additional magnetic layer [30]. The use of a trilayer structure with two ferromagnets with different magnetic anisotropies coupled by a Ta layer forming a so-called T-type structure has led to the observation of robust field-free switching [31–33].

In this paper we study the $Co_{20}Fe_{60}B_{20}$/Ta/$Co_{20}Fe_{60}B_{20}$ trilayer structure in order to determine the coupling via the Ta spacer and SOT induced magnetization switching of CoFeB. Similar to Ref. [31] Ta serves as the coupling layer, but in the presented case it also acts as a source of the spin current.

*lazarski@agh.edu.pl
†skowron@agh.edu.pl

 

By carefully selecting the CoFeB layer thicknesses, the deposition condition, and the thermal treatment, we are able to control the magnetic anisotropy. The interlayer exchange coupling (IEC) [34] across a Ta spacer is investigated using the ferromagnetic resonance (FMR) measurements. This coupling induces different magnetic orientations of two CoFeB layers, which results in a nontrivial dependence of the switching field and critical SOT induced current dependence as a function of Ta thickness.

## II. EXPERIMENT

All samples were magnetron sputtered on a thermally oxidized Si wafer with a wedged-shaped Ta layer deposited using a moving shutter technique. The investigated multilayer structure is as follows:

Ta(2)/$Co_{20}Fe_{60}B_{20}$(4)/Ta($t_{Ta}$)/$Co_{20}Fe_{60}B_{20}$(1.3)/MgO (3)/TaOx(2) (thickness in nanometers) with $t_{Ta}$ varying from 0 to 8 nm. The bottom (thicker) and the top (thinner) $Co_{20}Fe_{60}B_{20}$ layers exhibit in-plane (IMA) and perpendicular magnetic anisotropy (PMA), respectively. Additional multilayers with single FM layers and variable thicknesses of Ta or CoFeB were deposited: Ta(0 − 10)/$Co_{20}Fe_{60}B_{20}$5)/Ta(1) and Ta(5)/$Co_{20}Fe_{60}B_{20}$(0–10)/Ta(1) for resistivity analysis and PMA measurements using the anomalous Hall effect (AHE). Weak effective PMA of the top CoFeB layer was observed in the as-deposited state for a limited thickness of CoFeB around 1 nm. After annealing at 300 °C for 10 min, the range of CoFeB thicknesses for which effective PMA was found increased, which is confirmed by the evolution of the AHE signal in a half-stack with variable thickness of FM: Ta(5)/$Co_{20}Fe_{60}B_{20}$(0–2)/MgO(2)/Ta(1). The resistivity of CoFeB and Ta was determined in bilayers of variable thicknesses according to the model presented in Ref. [35]. After the deposition process, all samples were characterized by x-ray diffraction (XRD) and x-ray reflectivity measurements using a X'Pert-MPD diffractometer with a Cu anode to assist in controlling the thickness of particular layers in the system and phase analysis.

For the thinnest wedge thicknesses of $t_{Ta} < 2$ nm, the grazing incident angle profile measurements show no peaks. For $2 < t_{Ta} < 6$ nm, a broad peak corresponding to the amorphous Ta appears. Finally, for $t_{Ta} > 6$ nm the measurement results contain peaks that originate from a disoriented polycrystalline tetragonal $\beta$ phase [36]. For more details see the Supplemental Material [37].

For magnetotransport measurements, the Hall bars along with the rectangular stripes were fabricated using 385-nm projection lithography, ion-beam etching, and the liftoff process. The elements dimensions were: 10 $\mu$m × 100 $\mu$m for SOT dynamics measurements, 30 $\mu$m × 10 $\mu$m stripes for current induced magnetization switching and Hall bars, and 10 $\mu$m × 80 $\mu$m for AHE measurements. An example of the fabricated Hall bar with additional contact electrodes made of Al(20)/Au(30) is presented in Fig. 1. The long axes of the fabricated devices are perpendicular to the wedge direction, and the $t_{Ta}$ variation within a single device is below 0.05 nm.

The AHE was measured in a perpendicular magnetic field with constant current flowing through the long axis of the Hall bar. Spin-orbit torque ferromagnetic resonance (SOT-FMR)—with a rf signal of the constant frequency ($f$) applied where DC voltage was measured—was determined using the same electrodes (two-point) and perpendicular Hall electrodes (four-point) with the in-plane magnetic field ($H$) swept along a 45° axis with respect to the long axis of the stripe. In general, the stronger SOT-FMR signal is measured using the two-point method for in-plane magnetized CoFeB, whereas the four-point method is more suitable for CoFeB with effective perpendicular magnetic anisotropy Ref. [38].

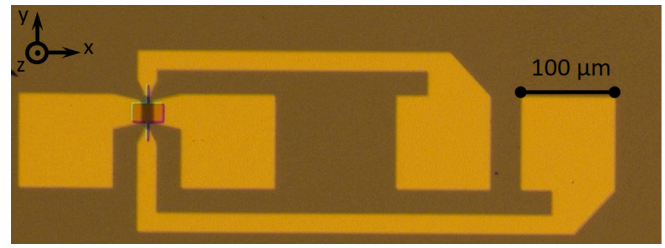


FIG. 1. Micrograph of the Hall-bar structure used for SOT current induced magnetization switching measurements.

## III. RESULT AND DISCUSSION

### A. Anomalous Hall effect

CoFeB and Ta layers resistivity determined in bilayers are as follows: $\rho_{Ta} = 170\ \mu\Omega$ cm and $\rho_{CoFeB} = 160\ \mu\Omega$ cm. The presence of the PMA in thin CoFeB was confirmed by the AHE measurements. The maximum coercivity ($H_C$) was found for $t_{CoFeB} = 1.3$–$1.5$ nm. Thinner (thicker) CoFeBs are characterized by perpendicular (in-plane) magnetic anisotropy, which is shown in Fig. 2(a). Figure 2(b) presents the AHE loops evolution of CoFeB/Ta/CoFeB trilayers as a function of the Ta spacer thickness.

Clearly, the magnetic behavior of the top CoFeB layer is modulated by the spacer thickness. For $t_{Ta}$ below 0.7 nm, the

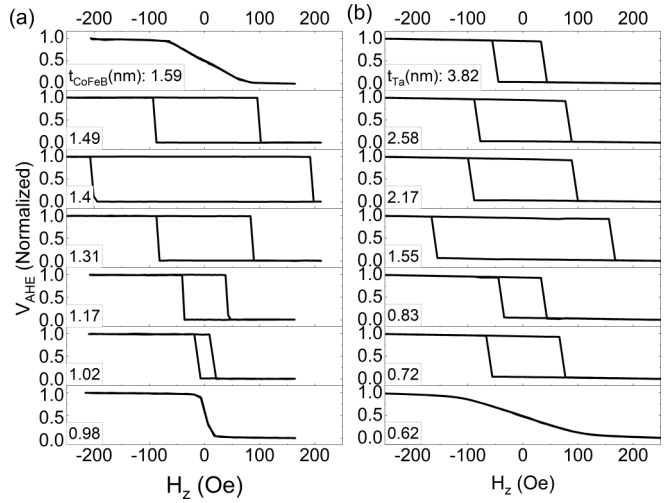


FIG. 2. AHE hysteresis loops measured in (a) a bilayer with a single FM as a function of CoFeB thickness: Ta(5)/CoFeB (0–2)/MgO(2)/Ta(1), (b) trilayers with two FM layers separated by different Ta spacer thicknesses: Ta(2)/CoFeB(5)/Ta(0–8) /CoFeB(1)/MgO(2)/Ta(1). Both samples were annealed at 300 °C.

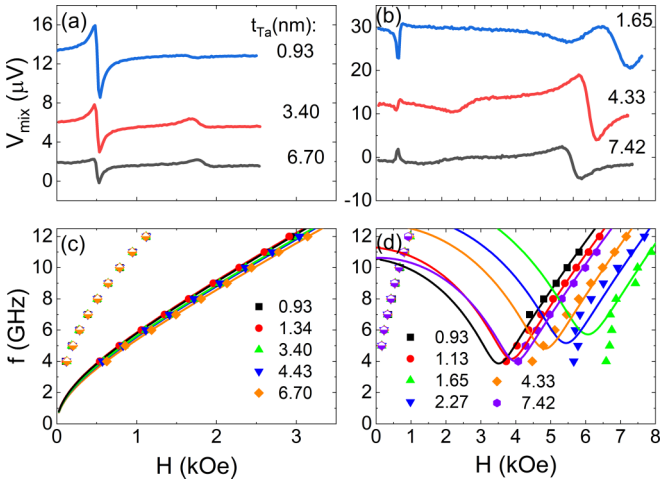


FIG. 3. Ferromagnetic resonance measurements on Hall-bar devices with different $t_{Ta}$'s. (a) and (b) show exemplary SOT-FMR curves for 8 GHz in as-deposited and 10 GHz in annealed states, respectively. The Kittel relation, i.e., the resonance frequency vs magnetic-field dependence of IMA CoFeB (open symbols) and PMA CoFeB (full symbols) for both cases are presented in (c) and (d). Macrospin simulation results are drawn with solid lines.

hard-axis closed hysteresis loop corresponding to the strong ferromagnetic coupling to the bottom in-plane magnetized CoFeB layer is measured. For thicker Ta the $H_C$ of the top CoFeB is modulated, which is a signature of the antiferromagnetic coupling of different energies as proposed in Ref. [39].

However, the magnetization switching process in micron-scale Hall bars is determined by the domain nucleation and propagation, therefore, precise determination of the coupling energy is challenging. Moreover, conventional magnetometry cannot be used for the determination of the IEC energy in the presented case where magnetic anisotropy axes of two CoFeB layers are orthogonal. For this purpose, we performed SOT-FMR measurements of the coupled CoFeB/Ta/CoFeB system.

### B. Interlayer exchange coupling

Representative SOT-FMR spectra measured for a trilayer in an as-deposited and annealed state are presented in Figs. 3(a) and 3(b). Two peaks in the magnetic-field domain correspond to the resonance frequency of the in-plane magnetized thick CoFeB (low field) and out-of-plane magnetized thin CoFeB (high field). The extracted signal $V_{mix}$ consists of two parts—symmetric and antisymmetric—which are modeled by Lorentz curves,

$$V_{mix} = V_S \frac{\Delta H^2}{\Delta H^2 + (H - H_0)^2} + V_A \frac{\Delta H (H - H_0)}{\Delta H^2 + (H - H_0)^2}, \quad (1)$$

where $V_S$ ($V_A$) is the magnitude of symmetrical (antisymmetrical) Lorentz curve, $\Delta H$ is the linewidth, and $H_0$ is the resonance field.

Figures 3(c) and 3(d) present the $f(H)$ dependencies measured for different thicknesses of the Ta spacers. Strong dependence of the resonance peak on $t_{Ta}$ is observed in the annealed sample, which indicates that the coupling is greatly enhanced after the thermal treatment [40]. It was found in the XRD measurements, that after the annealing process, the intensity of the Ta peak increases together with the appearance of the peak from CoFeB, which indicates an improvement of the crystallization process. Detailed crystallographic analysis is presented in the Supplemental Material [37].

The $f(H)$ dependence was analyzed using the macrospin model as follows. First, taking into account the saturation magnetization $M_S$ of each layer, magnetic anisotropy energy ($K$), and the coupling energy between them, the total energy term was minimized, which resulted in the orientation of the magnetization vector of two CoFeB layers. Next, the FMR frequency of each layer was calculated based on Smit-Beljers resonance formula, which resulted in two theoretical $f(H)$ dependencies Ref. [41].

It was assumed, that for the thickest Ta spacer, the IEC energy is negligibly small and the experimental points were fitted by adjusting the anisotropy energy alone. Parameters used in the modeling were as follows: $\mu_0 M_{S1} = 1.4$ and $\mu_0 M_{S2} = 0.5$ T for the bottom and top CoFeBs were measured using a vibrating sample magnetometer, the anisotropy energies were determined from an independent electrical transport measurement (anomalous Hall effect and magnetoresistance—see in detail in the Supplemental Material [37]): $K_{A1} = 5 \times 10^3$ and $K_{A2} = 1.75 \times 10^5$ J/m$^3$ for the bottom and top CoFeB layers, respectively. The magnetic anisotropy values of the bottom and top CoFeB layers correspond to the effective anisotropies of $K_{eff_1} = 7.73 \times 10^5$ and $K_{eff_2} = -7.58 \times 10^4$ J/m$^3$ based on Eq. (2),

$$K_{eff} = \frac{\mu_0 {M_s}^2}{2} - K_A, \quad (2)$$

where $\mu_0$ is the vacuum permeability.

Next, in order to model the experimental $f(H)$ dependencies for the entire range of $t_{Ta}$, the coupling was adjusted. However, it was found that changing the IEC energy [Fig. 4(b)] alone results in the values of an order of magnitude higher than in previous studies Refs. [42,43] and deviation of the FMR frequency of the thick CoFeB. Therefore, the best fits were obtained by adjusting both the coupling and the anisotropy energies for all $t_{Ta}$'s investigated. We note that neighboring layer thickness can influence the anisotropy of CoFeB as presented in Ref. [44]. In a similar material system it was found that the anisotropy field of the perpendicularly magnetized FeCoB layer was influenced by the Ta underlayer thickness [45], which was crucial for STT-magnetic random access memory (MRAM) cells based on a similar structure [46]. The detailed simulations based on the Landau-Lifshitz-Gilbert equation together with experimental data are presented in the Supplemental Material [37]. The simulation results are gathered in Figs. 4(a) and 4(b).

### C. SOT induced switching

After the analysis of the coupling energy, we now turn to the SOT induced switching experiments. Similar to the previous work [27] we used the HM both as a spacer and as a source of the spin current. Unlike in the Co/Pt/Co case where strong ferromagnetic coupling [47] and field-free magnetization switching [27] were observed, the CoFeB/Ta/CoFeB did not result in a field-free switching in the antiferromagnetic

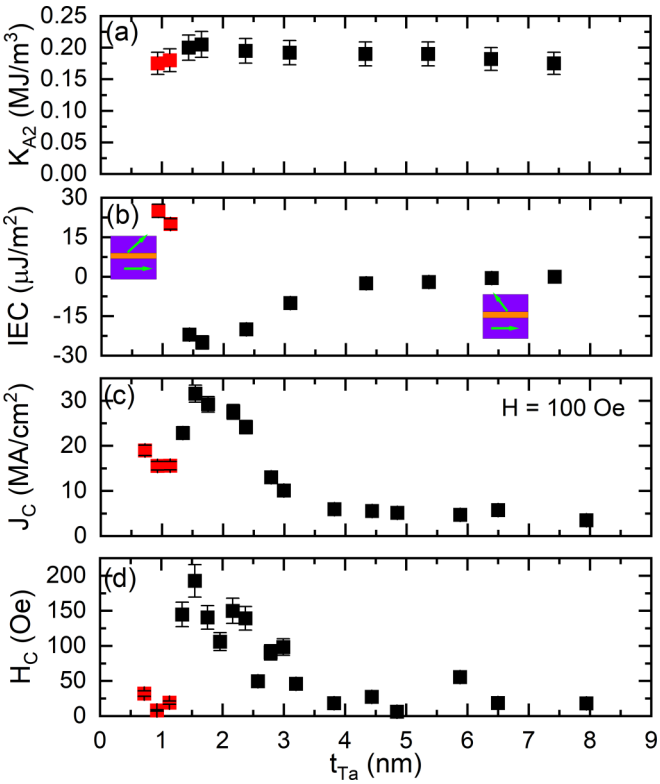


FIG. 4. Dependence of the magnetic anisotropy of the (a) top CoFeB-$K_{A2}$, (b) IEC energy via Ta spacer, (c) critical current density $J_C$, and the (d) top CoFeB coercive field $H_C$ as a function of $t_{Ta}$. The red point corresponds to the ferromagnetic IEC range.

coupling region. The example of the switching process with the assistance of the external magnetic field is presented in Fig. 5(a). The $J_C$ dependence on $t_{Ta}$ in the external field $H_x = 100$ Oe applied along the long axis of the Hall bar is presented in Fig. 4(c). The behavior closely resembles the coercive field dependence on $t_{Ta}$.

$J_C$ needed to switch the top CoFeB magnetization in the presence of an external magnetic field is increasing with decreasing Ta spacer thickness along with a rise in negative coupling energy until the transition to the ferromagnetic coupling for $t_{Ta} = 1.3$ nm occurs. The Hall-bar

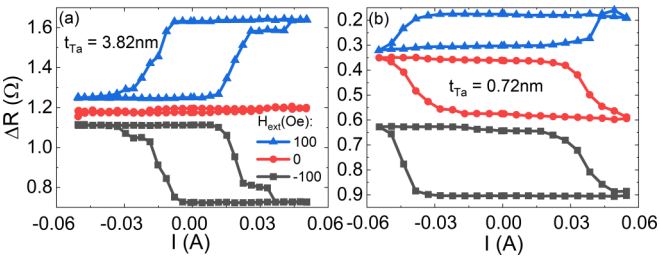


FIG. 5. SOT induced switching with (a) $t_{Ta}$ corresponding to the antiferromagnetic coupling and (b) ferromagnetic coupling in different external magnetic fields. Field-free switching is measured only for the sample characterized by the ferromagnetic coupling between two CoFeB electrodes. The offset is artificially added for clear viewing.

switches deterministically only in the in-plane magnetic field ($H = \pm 100$ Oe in the presented example). On the contrary, in the ferromagnetic coupling region, we observed current induced switching without any external magnetic field—Fig. 5(b)—but not fully complete—due to precisely selected ferromagnetic coupling (similar to Ref. [27]). The incomplete magnetization switching is most probably caused by the magnetic domain formation in the top CoFeB.

A ferromagnetic coupling appears only in a narrow Ta spacer thickness range. The switching process in this case may also be induced by the spin current from the bottom Ta layer. To further elucidate the field-free switching we calculated the current densities in each layer. For $t_{Ta} = 0.72$ nm, $J_C$ in the bottom Ta layer is $1.58 \times 10^{11}$ A/m$^2$, which is enough to switch the in-plane magnetized CoFeB layer [16]. Due to ferromagnetic coupling between two CoFeB layers, this leads to the magnetization change in thin CoFeB.

Alternatively, the spin current generated by the anomalous Hall effect [48] in thick CoFeB or its interface with Ta may also lead to a field-free switching of the perpendicular magnetized top CoFeB [28]. Nevertheless, in both scenarios due to a limited range of Ta spacer thickness for which the ferromagnetic coupling is observed, there is a need for an additional spin-current source layer in order to realize magnetic field-free switching.

## IV. SUMMARY

To sum up, the dynamics and the switching process in CoFeB/Ta/CoFeB trilayers with in-plane and perpendicular magnetic anisotropies of the two ferromagnets were investigated. The IEC, determined by the SOT-FMR technique was tuned by varying Ta spacer thickness and changes from ferromagnetic ($t_{Ta} < 1.3$ nm) to antiferromagnetic (1.3 nm $< t_{Ta}$). In the antiferromagnetic regime, a small external magnetic field is needed to achieve the SOT switching. In the ferromagnetic regime, however, the field-free SOT switching is obtained, but the range of change in resistance is slightly reduced. The implementation of two coupled FM layers with mixed anisotropies separated by a HM spacer enables determination of the fundamental SOT mechanisms and could advance the development of field-free SOT-MRAM devices in the future.

## ACKNOWLEDGMENTS

This work was supported by the National Science Centre, Grant No. UMO-2015/17/D/ST3/00500, Poland. W.S. acknowledges Grant No. LIDER/467/L-6/14/NCBR/2015 from the Polish National Centre for Research and Development. S.Ł., K.G., and T.S. acknowledge National Science Centre Grant No. Spinorbitronics UMO-2016/23/B/ST3/01430. Nanofabrication was performed at the Academic Centre for Materials and Nanotechnology of AGH University of Science and Technology. We would like to express our gratitude to Prof. F. Stobiecki, Dr. M. Czapkiewicz, and Dr. S. Ziętek for helpful discussions on data analysis.

[1] S. Ikiegawa, F. B. Mancoff, J. Janesky, and S. Aggarwal, Magnetoresistive random access memory: Present and future, IEEE Trans. Electron Devices **67**, 1407 (2020).

[2] S. Bhatti, R. Sbiaa, A. Hirohata, H. Ohno, S. Fukami, and S. N. Piramanayagam, Spintronics based random accessmemory: A review, Mater. Today **20**, 530 (2017).

[3] J. C. Slonczewski, Current-driven excitation of magnetic multilayers, J. Magn. Magn. Mater. **159**, L1 (1996).

[4] L. Berger, Emission of spin waves by a magnetic multilayer traversed by a current, Phys. Rev. B **54**, 9353 (1996).

[5] H. Ohno, D. Chiba, F. Matsukura, T. Omiya, E. Abe, T. Dietl, Y. Ohno, and K. Ohtani, Electric-field control of ferromagnetism, Nature (London) **408**, 944 (2000).

[6] S. Kanai. M. Yamanouchi, S. Ikeda, Y. Nakatani, F. Matsukura, and H. Ohno, Electric field-induced magnetization reversal in a perpendicular-anisotropy CoFeB-MgO magnetic tunnel junction, Appl. Phys. Lett. **101**, 122403 (2012).

[7] I. M. Miron, K. Garello, G. Gaudin, P.-J. Zermatten, M. V. Costache, S. Auffret, S. Bandiera, B. Rodmacq, A. Schuhl, and P. Gambardella, Perpendicular switching of a single ferromagnetic layer induced by in-plane current injection, Nature (London) **476**, 189 (2011).

[8] L. Liu, O. J. Lee, T. J. Gudmundsen, D. C. Ralph, and R. A. Buhrman, Current-Induced Switching of Perpendicularly Magnetized Magnetic Layers Using Spin Torque from the Spin Hall Effect, Phys. Rev. Lett. **109**, 096602 (2012).

[9] S. Emori, U. Bauer, S. M. Ahn, E. Martinez, and G. S. D. Beach, Current-driven dynamics of chiral ferromagnetic domain walls, Nature Mater. **12**, 611 (2013).

[10] S. Ikeda, J. Hayakawa, Y. Ashizawa, Y. M. Lee, K. Miura, H. Hasegawa, M. Tsunoda, F. Matsukura, and H. Ohno, Tunnel magnetoresistance of 604% at 300K by suppression of Ta diffusion in CoFeB/MgO/CoFeB pseudo-spin-valves annealed at high temperature, Appl. Phys. Lett. **93**, 082508 (2008).

[11] Y. Huai, F. Albert, P. Nguyen, M. Pakala, and T. Valet, Observation of spin-transfer switching in deep submicron-sized and low-resistance magnetic tunnel junctions, Appl. Phys. Lett. **84**, 3118 (2004).

[12] M. Nakayama, T. Kai, N. Shimomura, M. Amano, E. Kitagawa, T. Nagase, M. Yoshikawa, T. Kishi, S. Ikegawa, and H. Yoda, Spin transfer switching in TbCoFe/CoFeB/MgO/CoFeB/TbCoFe magnetic tunnel junctions with perpendicular magnetic anisotropy, J. Appl. Phys. **103**, 07A710 (2008).

[13] S. Ikeda, K. Miura, H. Yamamoto, K. Mizunuma, H. D. Gan, M. Endo, S. Kanai, J. Hayakawa, F. Matsukura, and H. Ohno, A perpendicular-anisotropy CoFeB-MgO magnetic tunnel junction, Nature Mater. **9**, 721 (2010).

[14] P. K. Amiri, Z. M. Zeng, J. Langer, H. Zhao, G. Rowlands, Y.-J. Chen, I. N. Krivorotov, J.-P. Wang, H. W. Jiang, J. A. Katine, Y. Huai, K. Galatsis, and K. L. Wang, Switching current reduction using perpendicular anisotropy in CoFeB-MgO magnetic tunnel junctions, Appl. Phys. Lett. **98**, 112507 (2011).

[15] K. Watanabe, B. Jinnai, S. Fukami, H. Sato, and H. Ohno, Shape anisotropy revisited in single-digit nanometer magnetic tunnel junctions, Nat. Commun. **9**, 663 (2018).

[16] L. Liu, C.-F. Pai, Y. Li, H. W. Tseng, D. C. Ralph, and R. A. Buhrman, Spin-torque switching with the giant spin hall effect of tantalum, Science **336**, 555 (2012).

[17] M. DC, R. Grassi, J.-Y. Chen, M. Jamali, D. R. Hickey, D. Zhang, Z. Zhao, H. Li, P. Quarterman, Y. Lv, M. Li, A. Manchon, K. A. Mkhoyan, T. Low, and J.-P. Wang, Room-temperature high spin–orbit torque due to quantum confinement in sputtered $Bi_XSe_{(1-x)}$ films, Nature Mater. **17**, 800 (2018).

[18] E. Grimaldi, V. Krizakova, G. Sala, F. Yasin, S. Couet, G. S. Kar, K. Garello, and P. Gambardella, Single-shot dynamics of spin–orbit torque and spin transfer torque switching in three-terminal magnetic tunnel junctions, Nat. Nanotechnol. **15**, 111 (2020).

[19] J. B. S. Mendes, R. O. Cunha, O. A. Santos, P. R. T. Ribeiro, F. L. A. Machado, R. L. Rodrîguez-Suárez, A. Azevedo, and S. M. Rezende, Large inverse spin Hall effect in the antiferromagnetic metal $Ir_{20}Mn_{80}$, Phys. Rev. B **89**, 140406(R) (2014).

[20] Y. Ou, S. Shi, D. C. Ralph, and R. A. Buhrman, Strong spin Hall effect in the antiferromagnet PtMn, Phys. Rev. B **93**, 220405(R) (2016).

[21] Y.-W. Oh, S.-H. C. Baek, Y. M. Kim, H. Y. Lee, K.-D. Lee, Ch.-G. Yang, E.-S. Park, K.-S. Lee, K.-W. Kim, G. Go, J.-R. Jeong, B-Ch. Mim, H.-W. Lee, K.-J. Lee, and B.-G. Park, Field-free switching of perpendicular magnetization through spin-orbit torque in antiferromagnet/ferromagnet/oxide structures, Nat. Nanotechnol. **11**, 878 (2016).

[22] S. Fukami, C. Zhang, S. DuttaGupta, A. Kurenkov, and H. Ohno, Magnetization switching by spin-orbit torque in an antiferromagnet-ferromagnet bilayer system, Nature Mater. **15**, 535 (2016).

[23] D. Wu, G. Yu, C.-T. Chen, S. A. Razavi, Q. Shao, X. Li, B. Zhao, K. L. Wong, C. He, Z. Zhang, P. K. Amiri, and K. L. Wang, Spin-orbit torques in perpendicularly magnetized $Ir_{22}Mn_{78}/Co_{20}Fe_{60}B_{20}/MgO$ multilayer, Appl. Phys. Lett. **109**, 222401 (2016).

[24] S. A. Razavi, D. Wu, G. Yu, Y.-C. Lau, K. L. Wong, W. Zhu, C. He, Z. Zhang, J. M. D. Coey, P. Stamenov, P. K. Amiri, and K. L. Wang, Joule Heating Effect on Field-Free Magnetization Switching by Spin-Orbit Torque in Exchange-Biased Systems, Phys. Rev. Appl. **7**, 024023 (2017).

[25] K. Grochot, Ł. Karwacki, S. Łazarski, W. Skowroński, J. Kanak, W. Powroźnik, P. Kuświk, M. Kowacz, F. Stobiecki, and T. Stobiecki, Current-Induced Magnetization Switching of Exchange-Biased NiO Heterostructures Characterized by Spin-Orbit Torque, Phys. Rev. Appl. **15**, 014017 (2021).

[26] Y. Liu, B. Zhou, and J.-G. Zhu, Field-free Magnetization Switching by Utilizing the Spin Hall Effect and Interlayer Exchange Coupling of Iridium, Sci. Rep. **9**, 325 (2019).

[27] S. Łazarski, W. Skowroński, J. Kanak, Ł. Karwacki, S. Ziętek, K. Grochot, T. Stobiecki, and F. Stobiecki, Field-Free Spin-Orbit Torque Switching in Co/Pt/Co Multilayer with Mixed Magnetic Anisotropies, Phys. Rev. Appl. **12**, 014006 (2019).

[28] S-H. C. Baek, V. P. Amin, Y.-W. Oh, G. Go, S.-J. Lee, G.-H. Lee, K.-J. Kim, M. D. Stiles, B.-G. Park, and K.-J. Lee, Spin currents and spin-orbit torques in ferromagnetic trilayers, Nature Mater. **17**, 509 (2018).

[29] M. Wang, W. Cai, D. Zhu, Z. Wang, J. Kann, Z. Zhao, K. Cao, Z. Wang, Y. Zhang, T. Zhang, C Park, J.-P. Wang, A. Fert, and W. Zhao, Field-free switching of a perpendicular magnetic tunnel junction through the interplay of spin-orbit and spin-transfer torques, Nat. Electron. **1**, 582 (2018).

[30] V. Krizakova, K. Garello, E. Grimaldi, G. S. Kar, and P. Gambardella, Field-free switching of magnetic tunnel junctions

driven by spin-orbit torques at sub-ns timescales, Appl. Phys. Lett. **116**, 232406 (2020).

[31] W. J. Kong, C. H. Wan, X. Wang, B. S. Tao, L. Huang, C. Fang, C. Y. Guo, Y. Guang, M. Irfan, and X. F. Han, Spin-orbit torque switching in a T-type magnetic configuration with current orthogonal to easy axes, Nat. Commun. **10**, 233 (2019).

[32] G. Yu, P. Upadhyaya, Y. Fan, J. G. Alzate, W. Jiang, K. L. Wong, S. Takei, S. A. Bender, L.-T. Chang, Y. Jiang, M. Lang, J. Tang, Y. Wang, Y. Tserkovnyak, P. K. Amiri, and K. L. Wang, Switching of perpendicular magnetization by spin-orbit torques in the absence of external magnetic fields, Nat. Nanotechnol. **9**, 548 (2014).

[33] L. You, O.-J. Lee, D. Bhowmik, D. Labanowski, J. Hong, J. Bokor, and S. Salahuddin, Switching of perpendicularly polarized nanomagnets with spin orbit torque without an external magnetic field by engineering a tilted anisotropy, Proc. Natl. Acad. Sci. USA **112**, 10310 (2015).

[34] S. S. P. Parkin, N. More, and K. P. Roche, Oscillations in Exchange Coupling and Magnetoresistance in Metallic Superlattice Structures: Co/Ru, Co/Cr, and Fe/Cr, Phys. Rev. Lett. **64**, 2304 (1990).

[35] M. Kawaguchi, D. Towa, Y.-C. Lau, S. Takahashi, and M. Hayashi, Anomalous spin Hall magnetoresistance in Pt/Co bilayers, Appl. Phys. Lett. **112**, 202405 (2018).

[36] M. Cecot, Ł. Karwacki, W. Skowroński, J. Kanak, J. Wrona, A. Żywczak, L. Yao, S. van Dijken, J. Barnaś, and T. Stobiecki, Influence of intermixing at the Ta/CoFeB interface on spin Hall angle in Ta/CoFeB/MgO heterostructures, Sci. Rep. **7**, 968 (2017).

[37] See Supplemental Material at http://link.aps.org/supplemental/10.1103/PhysRevB.103.134421 for more details.

[38] M. Harder, Y. Gui, and C.-M. Hu, Electrical detection of magnetization dynamics via spin rectification effects, Phys. Rep. **661**, 1 (2016).

[39] S. S. P. Parkin, Systematic Variation of the Strength and Oscillation Period of Indirect Magnetic Exchange Coupling through the *3d*, *4d*, and *5d* Transition Metals, Phys. Rev. Lett. **67**, 3598 (1991).

[40] Y. Liu, L. Hao, and J. Cao, Effect of annealing conditions on the perpendicular magnetic anisotropy of Ta/CoFeB/MgO multilayers, AIP Adv. **6**, 045008 (2016).

[41] S. Serrano-Guisan, W. Skowroński, J. Wrona, N. Liebing, M. Czapkiewicz, T. Stobiecki, G. Reiss, and H. W. Schumacher, Inductive determination of the optimum tunnel barrier thickness in magnetic tunneling junction stacks for spin torque memory applications, J. Appl. Phys. **110**, 023906 (2011).

[42] C.-W. Cheng, C. H. Shiue, T.-I. Cheng, and G. Chern, Observation of parallel-antiparallel magnetic coupling in ultrathin CoFeB-MgO based structures with perpendicular magnetic anisotropy, J. Appl. Phys. **112**, 033917 (2012).

[43] K. Wang, L. Qian, S.-C. Ying, and G. Xiao, Manipulation of the interlayer exchange coupling in perpendicular magnetized thin films via tunable magnetic-layer and spacer thicknesses, Phys. Rev. B **102**, 144430 (2020).

[44] D. D. Lam, F. Bonell, S. Miwa, Y. Shiota, K. Yakushiji, H. Kubota, T. Nozaki, A. Fukushima, S. Yuasa, and Y. Suzuki, MgO overlayer thickness dependence of perpendicular magnetic anisotropy in CoFeB thin films, J. Korean Phys. Soc. **62**, 1461 (2013).

[45] V. Sokalski, M. T. Moneck, E. Yang, and J.-G. Zhu, Optimization of Ta thickness for perpendicular magnetic tunnel junction applications in the MgO-FeCoB-Ta system, Appl. Phys. Lett. **101**, 072411 (2012).

[46] D. C. Worledge, G. Hu, D. W. Abraham, J. Z. Sun, P. L. Trouilloud, J. Nowak, S. Brown, M. C. Gaidis, E. J. O'Sullivan, and R. P. Robertazzi, Appl. Phys. Lett. **98**, 022501 (2011).

[47] A. Bonda, S. Uba, L. Uba, W. Skowroński, T. Stobiecki, and F. Stobiecki, Laser-induced magnetization precession parameters dependence on Pt spacer layer thickness in mixed magnetic anisotropies Co/Pt/Co trilayer, J. Magn. Magn. Mater. **505**, 166702 (2020).

[48] S. Iihama, T. Tanihuchu, K. Yakushiji, A. Fukushima, Y. Shiota, S. Tsunegi, R. Hiramatsu, S. Yuasa, Y. Suzuki, and H. Kubota, Spin-transfer torque induced by the spin anomalous Hall effect, Nat. Electron. **1**, 120 (2018).